Low Temperature Physics/Fizika Nizkikh Temperatur, 2021, vol. 47, No. 9, pp. 819–829

Electronic spectra, topological states and impurity effects in graphene nanoribbons

Yuriy G. Pogorelov

IFIMUP-IN, Departamento de Física, Universidade do Porto, Porto, Portugal

Denis Kochan

Institute of Theoretical Physics, University of Regensburg, Regensburg, Germany

Vadim M. Loktev

Bogolyubov Institute for Theoretical Physics of the National Academy of Sciences of Ukraine, Kyiv 03680, Ukraine

National Technical University of Ukraine "Igor Sikorsky Kyiv Polytechnic Institute", Kyiv 03056, Ukraine
E-mail: ypogorel@fc.up.pt; denis.kochan@ur.de; vloktev@bitp.kiev.ua

Received April 12, 2021, published online July 26, 2021

We consider the finite ribbons of graphene with two principal orientations, zigzag and armchair, of their edges to study in detail impurity effects on their edge states. An alternative to the known description of quasiparticle states in terms of transversal standing waves is proposed in the recurrence relations for their spectra vs discrete numbers of atomic chains in the ribbon, permitting to simplify the Green function approach to the disorder effects in these systems. The derived analysis shows the microscopic mechanisms of perturbation by different types of impurities on low energy states and clarifies how the stability of topological states in zigzag systems to disorder is related to the discrete amplitudes of these states across the ribbon. An opposite possibility for Mott localization under local impurity perturbations is found for armchair type nanoribbons but at special values of their width.

Keywords: graphene nanoribbons, topological states, impurity disorder, Lifshitz model, Anderson model.

1. Introduction

A variety of physical structures result from the specific triple topology of carbon valence links. Beyond the most common graphite and diamond 3D crystals, the discoveries of last decades include a sequence of fullerene molecules [1], going to the limit of carbon nanotubes [2], and, of course, the remarkable family of graphene atomic plane materials [3–6] with their derivatives [7]. For an extended guide through the nanocarbon jungle see the review of D. Tománek [8].

Especially, a lot of interest was attracted by the topological electronic states formed at the edges of finite cuts of the graphene plane [9, 10]. These show a remarkable sensitivity to the lattice orientation of the nanoribbon terminal edges. In particular, the possibility of topological protection of such edge states against the back-scattering, which gives rise to 1D metallic conductivity, was a subject of the intense experimental and theoretical studies [11–14]. Theory connected such stability with the specifics of the Berry phase dependence of the graphene Bloch states (resulting from the three-fold local symmetry of graphene links) on the wave vector orientation.

The graphene nanoribbons (GNR's) cut along its two principal crystalline axes, zigzag and armchair directions, are an important class of finite graphene systems. Correspondingly, the related GNR types are commonly lumped the names — zigzag graphene nanoribbons (ZGNR's) and armchair graphene nanoribbons (AGNR's). Although both graphene descendants, their different edge terminations endow them with strikingly different physical properties. First of all, the topological protection is observed for ZGNR's but not for AGNR's, and concomitantly, the quasiparticles spectra of AGNR's are sensitive to the number of atomic chains across the ribbon (semiconducting vs metallic AGNR's). This is another GNR's specifics (beyond

the sensitivity to the edge orientation) and, notably, it is absent in the ZGNR case, marking another qualitative distinction between the two GNR types.

The most complete analytic description of electronic states and their energy spectra for pure GNR's was obtained within the approach of standing waves in transversal wave numbers [15, 16], referred to in what follows as Wakabayashi–Sasaki–Nakanishi–Enoto (WSNE) approach [17].

The stability of electronic states in GNR's to disorder, particularly to the disorder by different types of impurities, was broadly discussed in various aspects, but the important issues of carriers lifetimes and the criteria for their localization were mostly treated by numerical methods [16, 18]. Therefore, it is of interest to consider these issues in a purely analytic way, within the general approach for disordered systems in terms of Green functions (GF's) [19, 20], permitting much more freedom to obtain various physical quantities. Such an analysis was done recently for the case of the plain 2D graphene with impurities [21, 22], and below we shall extend it for the GNR hosts, combining their original WSNE description with its alternatives developed here for easier matching to the GF schemes.

The paper is organized as follows, Sec. 2 includes the formulation of tight-binding Hamiltonians for ZGNR and AGNR types, and provides their diagonalization in terms of the longitudinal wave number k (along the GNR edge), leaving the transverse spatial direction lumped by the transverse (chain number) index j. A substantial part of Sec. 2 is devoted to the recurrence analysis for the corresponding secular determinants that give rise to the GNR eigenstates and their eigenvalues. Spectral analyzes and the dispersion laws for both GNR types are further investigated in Sec. 3, including, in particular, the quasi-dispersionless edge modes for ZGNR's and Dirac-like 1D nodes in AGNR's. Section 4 uses the obtained spectral data to build the GF's for each GNR type, especially the most relevant locator GF's for the terminal sites located at the GNR edges. The obtained GF's are further processed in Sec. 5 where perturbation Hamiltonians corresponding to different impurity perturbation models (Lifshitz and Anderson) and impurity positions (top and bridge) in GNR's are analyzed within the T matrix approximation. This analyzes shows how the stability of the ZGNR edge modes against the impurity disorder results from their specific dispersion laws, in contrast to the high sensibility of the AGNR Dirac-like states to such disorder. Finally, a brief discussion of the obtained results and their relation to the more general context of graphene physics is given in Sec. 6.

This work is dedicated to the glowing memory of M. I. Kaganov and to his great contribution to the theory of metals, particularly to our present understanding of the relations between the topology of electronic states in metals and their observable characteristics [23, 24].

2. Hamiltonian and secular determinants

A graphene nanoribbon can be considered as a set of M chains, each consisting of N (supposed $N \gg M$) 1D segments. Each segment contains two types of atomic sites, sublattices, and therefore the respective local electronic states in the nth segment of mth chain are represented by the second quantization operators $a^{\dagger}_{m,n}$ and $b^{\dagger}_{m,n}$ (see Fig. 1). Longitudinal periodicity is imposed through the Born-von Karman conditions connecting the 1st and Nth segments within each chain. The electronic dynamics of

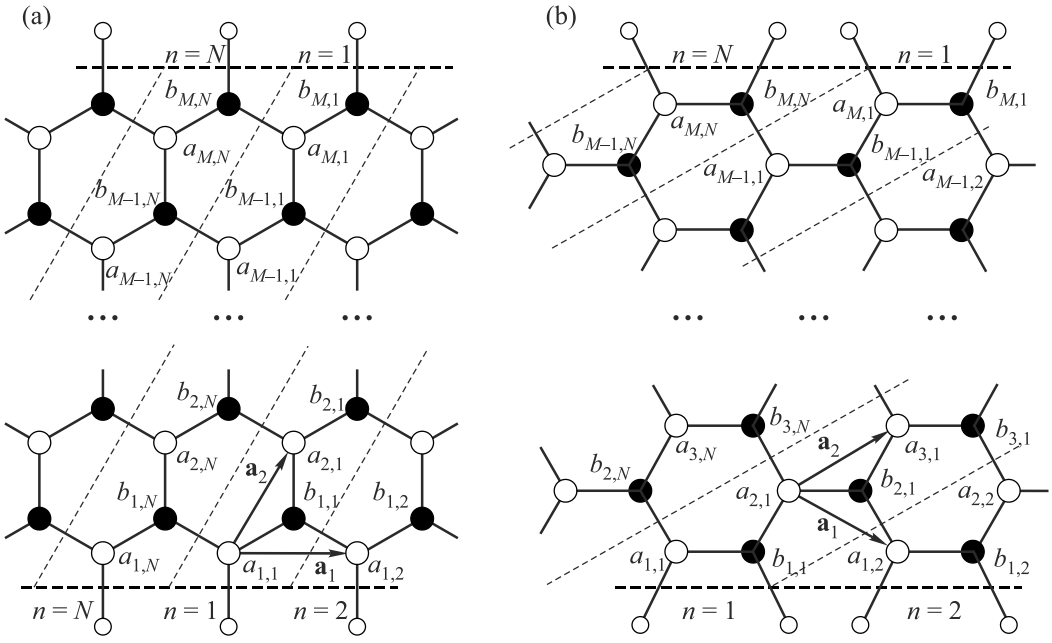

Fig. 1. Graphene nanoribbons for two orientations of their edges: (a) zigzag, along the lattice vector a_1, and (b) armchair, along $a_1 + a_2$. Dashed lines delimit the unit segments along a_2 with $2M$ atomic sites each, belonging to sublattice a (white) and b (black). The carbon dangling bonds at the edges are passivated by hydrogens (smaller circles).

such systems depend on the ribbon orientation with respect to the 2D graphene lattice vectors $\mathbf{a}_1$ and $\mathbf{a}_2$. There are distinguished ZGNR's extending along the $\mathbf{a}_1$ or $\mathbf{a}_2$ directions, and AGNR's extending along the $\mathbf{a}_1 \pm \mathbf{a}_2$ directions.

For a ZGNR with M chains and the nearest neighbor hopping t, the corresponding tight-binding Hamiltonian reads:

$$H^{(z,M)} = t\left\{\sum_{n=2}^{N}\left[\sum_{m=2}^{M-1} a_{m,n}^{\dagger}\left(b_{m,n}+b_{m,n-1}+b_{m-1,n}\right)+\right.\right.$$
$$\left.+a_{1,n}^{\dagger}\left(b_{1,n}+b_{1,n-1}\right)\right]+$$
$$\left.+\sum_{m=1}^{M} a_{m,1}^{\dagger}\left(b_{m,1}+b_{m,N}\right)+\text{h.c.}\right\}. \qquad (1)$$

Similarly, such Hamiltonian for an AGNR is:

$$H^{(a,M)} = t\left\{\sum_{n=1}^{N}\left[\sum_{m=2}^{M} a_{m,n}^{\dagger}\left(b_{m,n}+b_{m+1,n-1}+b_{m-1,n}\right)+\right.\right.$$
$$\left.+a_{1,n}^{\dagger}\left(b_{1,n}+b_{2,n-1}\right)\right]+$$
$$\left.+\sum_{m=1}^{M-1} a_{m,1}^{\dagger} b_{m+1,N}+\text{h.c.}\right\}. \qquad (2)$$

The last sums in Eqs. (1), (2) just generate longitudinal translation invariance, which suggests transition to the Fourier-transformed chain-wave operators. The longitudinal coordinates of $a_{m,n}$ and $b_{m,n}$ sites, as in Fig. 1(a) (in units of the graphene lattice constant $a = |\mathbf{a}_{1,2}|$) define this transform for the ZGNR case as:

$$\alpha_{m,k} = \frac{1}{\sqrt{2N}}\sum_{n=1}^{N} e^{i(2\pi k/N)(n+m/2-1/2)} a_{m,n},$$
$$\beta_{m,k} = \frac{1}{\sqrt{2N}}\sum_{n=1}^{N} e^{i(2\pi k/N)(n+m/2)} b_{m,n}, \qquad (3)$$

with the longitudinal wave number $k = 1, 2, \ldots, N$. The same for the AGNR case [as in Fig. 1(b)] reads:

$$\alpha_{m,k} = \frac{1}{\sqrt{2N}}\sum_{n=1}^{N} e^{i(2\pi k/N)\sqrt{3}(n+m/2+1/3)} a_{m,n},$$
$$\beta_{m,k} = \frac{1}{\sqrt{2N}}\sum_{n=1}^{N} e^{i(2\pi k/N)\sqrt{3}(n+m/2+2/3)} b_{m,n}. \qquad (4)$$

These transforms readily diagonalize the Hamiltonians, Eqs. (1), (2), in the k number. If the GNR length is macroscopically big, $N \to \infty$, we can pass to a quasi-continuous momentum variable: $2\pi k / N \to k$, defined within $0 < k < 2\pi$ (in a^{-1} units). Also, for a simplicity, the energy ε will be measured in units of t.

Then the system dynamics in the transversal m index can be considered at a fixed k, but in a specific way for each type of nanoribbons. The known analytic WSNE approach [15–17] is based on taking eigenstates at given k as standing waves in the transversal q momentum, subject to specific edge conditions for each GNR type. Their solution results quite simple for the AGNR case but more complicated for the ZGNR case, where a non-trivial coupling between the k and q momenta requires numerical calculation to obtain the final spectral data. This would also set difficulties for the further analytic studies of disorder effects on the most interesting ZGNR topological edge modes. Here we develop an alternative approach to the GNR systems, based directly on their m indices. It reproduces the WSNE results for pure GNR's electronic states and their spectra but permits a simpler treatment of disorder effects in the ZGNR case. At the same time, the WSNE approach is found easier for this purpose in the AGNR case.

2.1. Zigzag case

Thus, the transformed ZGNR case Hamiltonian from Eq. (1) reads:

$$H^{(z,M)} = \sum_{k}\left[\sum_{m=2}^{M}\left(\gamma_k \alpha_{m,k}^{\dagger}\beta_{m,k} + \alpha_{m,k}^{\dagger}\beta_{m-1,k}\right)+\right.$$
$$\left.+\gamma_k \alpha_{1,k}^{\dagger}\beta_{1,k}+\text{h.c.}\right], \qquad (5)$$

with the phase factor $\gamma_k = 2\cos\frac{k}{2}$. It can be also presented as

$$H^{(z,M)} = \sum_{k} \psi_k^{\dagger} \hat{H}^{(z,M)} \psi_k,$$

involving the row-vectors of chain-wave operators, $\psi_k^{\dagger} = \left\{\alpha_{1,k}^{\dagger}, \beta_{1,k}^{\dagger}, \ldots, \alpha_{M,k}^{\dagger}, \beta_{M,k}^{\dagger}\right\}$ (and the respective column-vectors ψ_k), and the $2M \times 2M$ matrix:

$$\hat{H}^{(z,M)} = \begin{pmatrix} 0 & \gamma_k & 0 & 0 & \ldots & 0 \\ \gamma_k & 0 & 1 & 0 & \ldots & 0 \\ 0 & 1 & 0 & \gamma_k & \ldots & 0 \\ 0 & 0 & \gamma_k & 0 & 1 & \ldots \\ \ldots & \ldots & \ldots & \ldots & \ldots & \ldots \\ 0 & \ldots & 0 & 1 & 0 & \gamma_k \\ 0 & \ldots & 0 & 0 & \gamma_k & 0 \end{pmatrix}, \qquad (6)$$

that is tridiagonal with alternating γ_k and unit elements along the side diagonals and zeros on the main diagonal.

Let us consider the secular determinant, $Z_M = \det(\varepsilon - \hat{H}^{(z,M)})$, of the tridiagonal $2M \times 2M$ matrix:

$$Z_M = \begin{vmatrix} \varepsilon & -\gamma_k & 0 & 0 & \ldots & 0 \\ -\gamma_k & \varepsilon & -1 & 0 & \ldots & 0 \\ 0 & -1 & \varepsilon & -\gamma_k & \ldots & 0 \\ 0 & 0 & -\gamma_k & \varepsilon & -1 & \ldots \\ \ldots & \ldots & \ldots & \ldots & \ldots & \ldots \\ 0 & \ldots & 0 & -1 & \varepsilon & \gamma_k \\ 0 & \ldots & 0 & 0 & \gamma_k & \varepsilon \end{vmatrix}, \qquad (7)$$

and then the sequence of such Z_M for $M = 1, 2, \ldots$.

Evidently, $Z_1 = \varepsilon^2 - \gamma_k^2$, and yet formally $Z_0 = 1$. The general form of any term in this sequence can be found from recurrence relations between a given Z_M and some lower order determinants.

Thus, Z_M given by Eq. (7) is expanded through its two 2nd order minors. The first of them, $Z_M^{(1,2;1,2)}$ (with excluded the rows 1, 2 and the columns 1, 2 from Z_M), equals just Z_{M-1} and has the cofactor Z_1 and the second, $Z_M^{(1,2;1,3)}$ (excluded the rows 1, 2 and the columns 1, 3), has the cofactor ε resulting in:

$$Z_M = Z_1 Z_{M-1} + \varepsilon Z_M^{(1,2;1,3)} \tag{8}$$

(while the $Z_M^{(1,2;2,3)}$ minor has zero cofactor and does not contribute).

We notice that Eq. (8) already gives the recurrence from Z_M down to Z_{M-1}, while the resting 2nd order minor $Z_M^{(1,2;1,3)}$ is expressed as:

$$Z_M^{(1,2;1,3)} = -Z_{M-1}^{(1;1)}, \tag{9}$$

that is through the 1st order minor of Z_{M-1} (excluding its row 1 and column 1) but entering here with the cofactor -1. And this latter is again expanded in its two 1st order minors to provide the next recurrence already to Z_{M-2}:

$$Z_{M-1}^{(1;1)} = \varepsilon Z_{M-2} - Z_{M-2}^{(1;1)}. \tag{10}$$

Iterating such expansion for $Z_{M-2}^{(1;1)}$ and so on, we come finally to the complete recurrence relation:

$$Z_M = Z_1 Z_{M-1} + \varepsilon^2 \sum_{j=1}^{M-1} (-1)^j Z_{M-1-j}. \tag{11}$$

Notably, Eq. (11) permits its explicit general solution:

$$Z_M = Z_1^M + \sum_{j=0}^{M-2} \sum_{k=1}^{\left[\frac{M-j}{2}\right]} (-1)^{M-j-k} \times$$

$$\times \binom{M-j-k-1}{k-1} \binom{j+k}{k} Z_1^j \varepsilon^{2k}, \tag{12}$$

where […] is the integer part and $\binom{m}{n}$ = m! = [n!(m..n)!] the binomial coefficient.

2.2. Armchair case

A similar approach to the armchair case is done with the Hamiltonian:

$$H^{(a,M)} = \sum_k \psi_k^\dagger \hat{H}^{(a,M)} \psi_k, \tag{13}$$

where ψ_k are the same vectors as before, but now $\hat{H}^{(a,M)}$ is the $2M \times 2M$ matrix which is tridiagonal in 2×2 blocs. The corresponding secular determinant $A_M = \det(\varepsilon - \hat{H}^{(a,M)})$ reads:

$$A_M = \begin{vmatrix} \hat{\varepsilon}_k & \hat{\eta}_k & 0 & 0 & \dots & 0 \\ \hat{\eta}_k & \hat{\varepsilon}_k & \hat{\eta}_k & 0 & \dots & 0 \\ 0 & \hat{\eta}_k & \hat{\varepsilon}_k & \hat{\eta}_k & \dots & 0 \\ 0 & 0 & \hat{\eta}_k & \hat{\varepsilon}_k & \hat{\eta}_k & \dots \\ \dots & \dots & \dots & \dots & \dots & \dots \\ 0 & \dots & 0 & \hat{\eta}_k & \hat{\varepsilon}_k & \hat{\eta}_k \\ 0 & \dots & 0 & 0 & \hat{\eta}_k & \hat{\varepsilon}_k \end{vmatrix}, \tag{14}$$

where the 2×2 blocks:

$$\hat{\eta}_k = \begin{pmatrix} 0 & -\eta_k \\ -\eta_{-k} & 0 \end{pmatrix}, \qquad \hat{\varepsilon}_k = \begin{pmatrix} \varepsilon & -\eta_{2k} \\ -\eta_{-2k} & \varepsilon \end{pmatrix},$$

involve the phase factors $\eta_k = e^{ik/2\sqrt{3}}$.

The recurrence relation for A_M is built up from six 2nd order minors upon its first two rows: $A_M^{(1,2;1,2)}$, $A_M^{(1,2;3,4)}$, $A_M^{(1,2;1,3)}$, $A_M^{(1,2;2,4)}$, $A_M^{(1,2;2,3)}$, and $A_M^{(1,2;1,4)}$. The straightforward contributions from $A_M^{(1,2;1,2)}$ and $A_M^{(1,2;3,4)}$ are, respectively, $A_1 A_{M-1}$ and A_{M-2} (here we define $A_1 = \varepsilon^2 - 1$ and set $A_0 = 1$). Next, the contribution from $A_M^{(1,2;1,3)}$ contains, besides A_{M-2} and its minor $A_{M-1}^{(1;1)}$ as in Eq. (9), yet its another minor $A_{M-1}^{(1;2)}$ (excluded 1st column and 2nd row from A_{M-1}). Equation (10) still applies for expansion of $A_{M-1}^{(1;1)}$, but this for $A_{M-1}^{(1;2)}$ appears different:

$$A_{M-1}^{(1;2)} = -\eta_{2k} A_{M-3} - A_{M-2}^{(2;1)}, \tag{15}$$

where $A_{M-2}^{(2;1)}$ is the complex conjugate to $A_{M-2}^{(1;2)}$. Continuing this by analogy for:

$$A_{M-2}^{(2;1)} = -\eta_{-2k} A_{M-4} - A_{M-3}^{(1;2)}, \tag{16}$$

we can close the recurrence for $A_{M-1}^{(1;2)}$:

$$A_{M-1}^{(1;2)} = -\eta_{2k} A_{M-3} + \eta_{-2k} A_{M-4} + A_{M-3}^{(1;2)}. \tag{17}$$

Then the contribution from $A_M^{(1,2;2,4)}$ is treated in a similar way and this leads to the full recurrence relation for A_M as follows:

$$A_M = A_1 A_{M-1} - (2A_1 + 2 + \zeta_k) A_{M-2} -$$

$$-2(A_1+1) \sum_{j=0}^{M-3} (-1)^j A_{M-3-j} - 2 \sum_{j=0}^{\left[\frac{M-3}{2}\right]} A_{M-3-2j} -$$

$$-\zeta_k \sum_{j=0}^{\left[\frac{M}{2}-2\right]} A_{M-4-2j} \tag{18}$$

(where $\zeta_k = 2\cos\frac{\sqrt{3}}{2}k$). Though this is much more involved than Eq. (11) and its general solution like that of Eq. (12) is not so straightforward, one can obtain from Eq. (18) a series of A_M for the subsequent M values, beginning from A_0 and A_1. Actually, they follow as:

$$A_2 = \varepsilon^4 - 4\varepsilon^2 + (2-\zeta_k),$$

$$A_3 = \varepsilon^6 - 7\varepsilon^4 + \varepsilon^2(11-2\zeta_k) - (5-2\zeta_k),$$

$$A_4 = \varepsilon^8 - 10\varepsilon^6 + \varepsilon^4(29-3\zeta_k) - \varepsilon^2(30-10\zeta_k) + (3-\zeta_k)^2,$$

$$A_5 = \varepsilon^{10} - 13\varepsilon^8 + 4\varepsilon^6(9-\zeta_k) - 8\varepsilon^4(10-3\zeta_k) + 4\varepsilon^2(19-5\zeta_k) - $$

$$-(10-3\zeta_k)(2-\zeta_k), \quad \ldots \qquad (19)$$

However, this problem is more suitably tackled with the WSNE approach [15, 17]. It gives the system of $2M$ eigenstates at given longitudinal momentum k as pairs of standing waves in consecutive values of transversal momentum:

$$q_j = \frac{\pi j}{M+1}, \quad j = 1, \ldots, M. \qquad (20)$$

These states are just the combinations (symmetric and antisymmetric in a and b sites) of 1D projected graphene states and their related eigenenergies will be analyzed below.

3. Quasiparticle spectra of nanoribbons

3.1. Zigzag case

Now we are in position to describe the quasiparticle spectra for each nanoribbon type using the related secular equations, $Z_M = 0$ or $A_M = 0$. Generally, there are M roots for ε^2 (at a given k), giving $2M$ bands symmetric with respect to zero energy: M conduction bands, $\varepsilon_{j,k} > 0$, $j = 1, \ldots, M$ and M valence bands, $\varepsilon_{-j,k} = -\varepsilon_{j,k} < 0$.

Limiting ourselves to the positive bands, we notice that their spectra possess a mirror symmetry with respect to $k = \pi$, so the following consideration can be safely limited to the BZ half, $0 \le k \le \pi$. Then, a qualitative distinction of the two types of spectra will be seen below in that the ZGNR bands do not intersect within this range (except for their node at its limit, $k = \pi$), but such intersections occur in the AGNR case. Therefore, the ZGNR bands can be labeled in the ascending order of energy:

$$0 < \varepsilon_{1,k} < \varepsilon_{2,k} < \ldots < \varepsilon_{M,k},$$

while these in AGNR are more naturally labeled in the ascending order of transversal momentum as in Eq. (20).

The most important physical feature of the considered spectra is the behavior of the lowest energy mode, closest to the Fermi level (understood unbiased, zero, in what follows). And such modes are also qualitatively different for the ZGNR and AGNR cases.

Thus, from the general ZGNR solution, Eq. (12), it follows that the lowest mode reaches zero at $k = \pi$, where $\gamma_\pi = 0$ and correspondingly the secular determinant is factored here as:

$$Z_M = \varepsilon^2\left(\varepsilon^2 - 1\right)^{M-1}, \qquad (21)$$

resulting in $\varepsilon_{1,\pi} = 0$. Then the dispersion of the lowest mode in the vicinity of $k = \pi$ is found from the expansion of Eq. (12) up to the 1st order in ε^2:

$$Z_M \approx (-1)^M\left[\gamma_k^{2M} - \varepsilon^2\left(1 + M\gamma_k^{2M-2}\right)\right], \qquad (22)$$

and since $\gamma_k \approx \pi - k$ here, the lowest mode dispersion is well approximated as:

$$\varepsilon_{1,k} \approx |k-\pi|^M. \qquad (23)$$

Such highly non-linear dispersion law for the two middle modes, $\pm\varepsilon_{1,k}$ near their joining at the Fermi level is the main spectral distinction of ZGNR vs the common linear dispersion of the plain 2D graphene near its Dirac points, permitting us to refer these modes as special. They assure the gapless (semi-metallic) type of electronic spectrum for any ZGNR width M and the approximation given by Eq. (23) applies as far as $|k-\pi| \ll 1$, while their evolution farther from $k = \pi$ is discussed below.

Another root of Eq. (21) indicates that the remaining (non-special) modes form the above mentioned $(M-1)$ fold node at $k = \pi$: $\varepsilon_{j,\pi} = 1$ for all $2 \le j \le M$. Their further development along BZ can be described by the general WSNE solution [17], using the 2D graphene dispersion law:

$$\varepsilon_{j,k} = \sqrt{1 + \gamma_k \cos q_j + \gamma_k^2}, \qquad (24)$$

with q_j chosen as the $(M+1-j)$th root of the equation:

$$\sin qM + \gamma_k \sin q(M+1) = 0, \qquad (25)$$

which just presents the aforementioned coupling between the k and q momenta in ZGNR. So, the formula by Eq. (24) cannot be used straightforwardly but requires first to find numerically all the roots of Eq. (25) for each k, while it results in the same dispersion laws as from the recursive solution by Eq. (12).

Next, the recursive solution for the special $\varepsilon_{1,k}$ mode describes continuously its transition in k from the peculiar regime given by Eq. (23) to the WSNE solution by Eq. (24) (see Fig. 2), while the latter is only defined for $k < k_c = \arccos[M/2(M+1)]$ and requires the use of an alternative set of equations for $k > k_c$.

In our approach, this transition occurs within the $\Delta k \sim (\ln M)/M$ interval near the 1D "Dirac point" $k = 2\pi/3$ (see Fig. 2), qualitatively agreeing with the WSTE transition: $\Delta k \sim k_c - 2\pi/3$.

For each eigenmode $\varepsilon_{j,k}$, the related eigenvector $\Phi^{(j,k)} = \{\phi_1^{(j,k)}, \phi_2^{(j,k)}, \ldots, \phi_{2M}^{(j,k)}\}$ (normalized to unity) has its amplitude $\phi_l^{(j,k)}$ on the lth position along each unit segment so that an odd, $l = 2m-1$, relates to the a type sites and an even, $l = 2m$, to the b type sites from the mth chain [see Fig. 1(a)]. It should solve the equation of motion:

$$\left(\varepsilon_{j,k} - \hat{H}^{(z,M)}\right)\Phi^{(j,k)} = 0. \qquad (26)$$

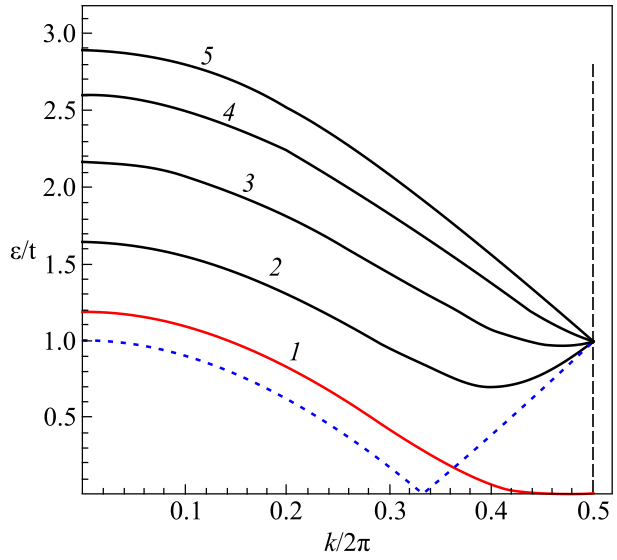

Fig. 2. Energy dispersion of the zigzag nanoribbon modes vs longitudinal momentum k. The special mode $\varepsilon_{1,k}$ (solid red line) is compared with the non-special $\varepsilon_{j,k}$, $2 \le j \le M$ (solid black lines), here for $M = 5$. The Dirac mode ε_D of 2D graphene, obtained by a cut along the Γ-K line of its BZ (blue dashed line), crosses the special mode near the transition point k_c [discussed after Eq. (25)]. In the limit of $M \to \infty$, the special mode approaches ε_D along $k < 2\pi/3$ and approaches zero along $k > 2\pi/3$. The negative, energy mirrored valence band modes are not shown.

In particular, for the special mode $\varepsilon_{1,k}$ with longitudinal momenta satisfying $|\gamma_k| \ll 1$ (a focus for interesting physics around the unbiased Fermi level), the odd amplitudes of $\Phi^{(1,k)}$ (a type sites) are found to decay exponentially from their maximum initial value, $\phi_1^{(1,k)}$, inwards the nanoribbon as:

$$\phi_{2m-1}^{(1,k)} \approx (-1)^{m-1}\gamma_k^{m-1}\phi_1^{(1,k)}. \tag{27}$$

In contrary, the even amplitudes (b type sites) begin from an exponentially small initial value $\phi_2^{(1,k)} = (\varepsilon_{1,k}/\gamma_k)\phi_1^{(1,k)}$ and grow as

$$\phi_{2m}^{(1,k)} \approx \gamma_k^{-m}\phi_2^{(1,k)}, \tag{28}$$

until reaching the maximum $\phi_{2M}^{(1,k)} = \phi_1^{(1,k)}$ on the other edge of the nanoribbon. From the normalization condition, $\sum_{l=1}^{2M}\left[\phi_l^{(1,k)}\right]^2 = 1$, we find the edge value:

$$\phi_1^{(1,k)} \approx \sqrt{\frac{1-\gamma_k^2}{2}}. \tag{29}$$

The resulting sharp dominance of the edge amplitudes of the eigenmode $\varepsilon_{1,k}$ at $|\gamma_k| \ll 1$ permits us to refer in what follows that mode as the edge mode.

In the limit of $M \gg 1$, the dispersion laws for the remaining $M-1$ modes, found from either Eq. (12) or from Eqs. (24), (25), tend to cover the uniform 1D projections of 2D graphene spectrum.

3.2. Armchair case

For the alternative of AGNR's, already their spectra found from the examples in Eq. (19) differ significantly from the above ZGNR case. Their most general form is given in the WSNE approach by simple uniform 1D projections of the 2D graphene spectrum at transverse momentum values q_j by Eq. (20):

$$\varepsilon_{j,k} = \sqrt{1+\zeta_k\gamma_{2q_j}+\gamma_{2q_j}^2}, \tag{30}$$

for conduction bands (and $-\varepsilon_{j,k}$ for valence bands). This leads to the general form of respective secular determinant:

$$A_M = \prod_{j=1}^{M}\left(\varepsilon^2 - \varepsilon_{j,k}{}^2\right), \tag{31}$$

which is readily verified to match all the particular forms from Eq. (19).

Also the general form of eigenstates associated with these modes are the transversal standing waves [17] having their amplitudes:

$$\phi_l^{(j,k)} = \frac{(-1)^l e^{i(-1)^l\varphi_{j,k}}}{\sqrt{M+1}}\sin m_l q_j, \tag{32}$$

where the phases are defined by the relation

$$\tan 2\varphi_{j,k} = \frac{\sin\frac{\sqrt{3}k}{2}}{\gamma_{2q_j}+\cos\frac{\sqrt{3}k}{2}},$$

the parity $(-1)^l$ of lth position again defines its a or b type and $m_l = \left[\frac{l+1}{2}\right]$ is the number of chain to which this position belongs.

The first notable feature of Eq. (30) is that it admits gapless modes if the AGNR width satisfies the condition [15]:

$$(M+1) \bmod 3 = 0. \tag{33}$$

For such a width, $M = 3r-1$, the modes with $j = 2r$ reach zero at the BZ edge $k = 0$ as:

$$\varepsilon_{2r,k} = 2\left|\sin\frac{\sqrt{3}k}{4}\right| \approx \frac{\sqrt{3}}{2}|k| \tag{34}$$

[see Figs. 3(a) and 3(d)], and those with $j = r$ reach zero at the opposite BZ edge $k = 2\pi$ as:

$$\varepsilon_{r,k} = 2\left|\cos\frac{\sqrt{3}(2\pi-k)}{4}\right| \approx \frac{\sqrt{3}}{2}|2\pi-k|. \tag{35}$$

The dispersion laws by Eqs. (34), (35) formally coincide with the standard linear dispersion near the Dirac points of 2D graphene, and hence they can be seen as definitions of effective 1D Dirac points in AGNR spectra.

Notably, the strict selection rule, Eq. (33) defines an important difference between AGNR and its ZGNR counterpart. Also, the striking difference between the gapless

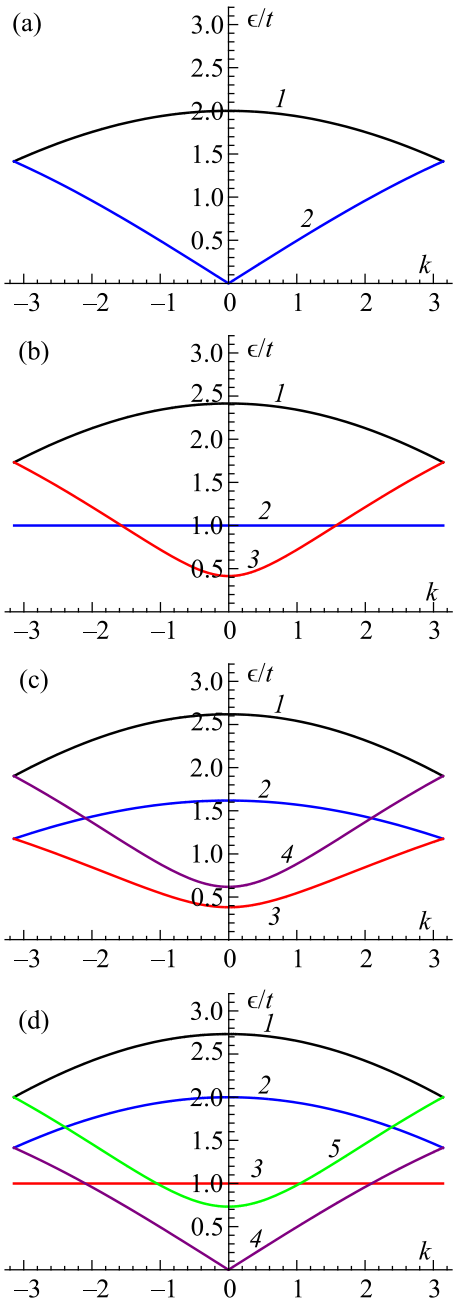

Fig. 3. Energy bands in AGNR at M: 2 (a), 3 (b), 4 (c), and 5 (d), showing Dirac-like modes for $M = 2.5$ and flat saddle-point modes for $M = 3.5$.

spectra represented by Eqs. (23) and (34), (35) underlines the high sensitivity of the GNR quasiparticle spectra to their edge orientations.

For all the M values that do not satisfy Eq. (33), the AGNR spectra display finite energy gaps.

Another peculiar feature of the spectra by Eq. (30) is the possibility for fully dispersionless modes at any odd AGNR width, $M = 2r-1$, realized then for $j = r$ as $\varepsilon_{p,k} \equiv 1$ [see Figs. 3(b) and 3(d)]. This occurs if a q projection exactly fits through two neighbor M points of 2D graphene BZ and, since those relate to saddle points of the graphene energy surface, such modes can be also referred to saddle modes.

Despite the AGNR saddle mode flatness looks similar to that of the ZGNR edge mode by Eq. (23), there is a radical difference in their amplitude profiles. For the AGNR saddle mode $\Phi^{(p,k)}$, it is essentially defined only by the parities of the position number l and the related chain number m_l:

$$\phi_l^{(p,k)} = \frac{(-1)^l}{\sqrt{M+1}} \begin{cases} e^{i(-1)^l \frac{\sqrt{3}}{4}k}, & \text{for } m_l \text{ odd}, \\ 0, & \text{for } m_l \text{ even}, \end{cases} \tag{36}$$

in contrast to the exponential localization of the ZGNR edge mode $\Phi^{(1,k)}$ by Eqs. (27), (28).

4. Green functions

4.1. Zigzag nanoribbon

Our main target is a study of disorder-induced effects on the nanoribbon lowest energy bands, we do that by employing the common GF approach applied separately to the ZGNR and AGNR cases. To begin with, we use the result for the ZGNR by Eq. (12), from which one can obtain the most relevant diagonal elements of the underlying GF matrix,

$$\hat{G}^{(z,M)} = \left(\varepsilon - \hat{H}^{(z,M)}\right)^{-1}. \tag{37}$$

Considering the tridiagonal structure of the $2M \times 2M$ matrix $\hat{H}^{(z,M)}$, see Eq. (6), each jth diagonal element of $\hat{G}^{(z,M)}$ is expressed as a combination of Z_M and its 1st order minors, specific for even or odd j:

$$G_{j,j}^{(z,M)} = \frac{Z_m^{(1;1)} Z_{M-m}}{Z_M}, \qquad \text{for } j = 2m,$$

$$G_{j,j}^{(z,M)} = \frac{Z_m Z_{M-m}^{(1;1)}}{Z_M}, \qquad \text{for } j = 2m+1. \tag{38}$$

Here in the numerators, each Z comes straightforwardly from Eq. (12), while the 1st order minor can be combined from the two subsequent Z's. Thus, for $j = 2m$, the factor Z_{M-m} comes straightforwardly while $Z_m^{(1;1)}$ is expressed from Eqs. (8), (9) as:

$$Z_m^{(1;1)} = \frac{Z_1 Z_m - Z_{m+1}}{\varepsilon}. \tag{39}$$

Otherwise, for $j = 2m+1$, the Z_m is straightforward and $Z_{M-m}^{(1;1)}$ is expressed through Z_{M-m} and Z_{M-m+1}.

When focusing again on the low energy range of the edge mode $\varepsilon_{1,k}$ and since $\hat{G}^{(z,M)}$ is written in the position j indices, we consider the most relevant terminal element:

$$G_{1,1}^{(z,M)} = \frac{Z_M^{(1;1)}}{Z_M} = \frac{Z_1 Z_M - Z_{M+1}}{\varepsilon Z_M}, \tag{40}$$

where the difference in the numerator counts two double sums from Eq. (12), which at the end reduce just to a single sum (the $j = 0$ term):

$$Z_1 Z_M - Z_{M+1} = (-1)^M \sum_{l=1}^{[(M+1)/2]} B_{M-l}^{l-1} \left(-\varepsilon^2\right)^l. \quad (41)$$

The latter sum explicitly follows from the formula:

$$\sum_{l=0}^{n} B_{2n-l}^{l} x^l = \frac{2^{-(2n+1)}}{\sqrt{1+4x}} \left[(\sqrt{1+4x}+1)^{2n+1} + (\sqrt{1+4x}-1)^{2n+1} \right], \quad (42)$$

and then its expansion to the first order in the small parameter $x = -\varepsilon^2$, together with that by Eq. (21), leads to the simple result:

$$G_{1,1}^{(z,M)} \approx \frac{\varepsilon}{\varepsilon^2 - \varepsilon_{1,k}^2}. \quad (43)$$

This expression already permits us to analyze possible impurity effects on the underlying ZGNR edge modes.

4.2. Armchair nanoribbon

The construction of GF matrix for the AGNR system is yet simplified due to its full diagonalization by Eqs. (30)–(32). The corresponding GF matrix has only diagonal elements:

$$G_{j,j}^{(a,M)} = \frac{1}{\varepsilon - \varepsilon_{j,k}}, \quad (44)$$

but now, unlike the previous ZGNR case, the j indices already count the transversal momenta as by Eq. (20) and also their opposites $-j$ ($2M$ altogether).

Besides this, for consideration of local impurity perturbations, we should yet to define the eigenmode operators $A_{j,k}$ and $A_{-j,k}$, expanded in the position indexed operators $\alpha_{m,k}$ and $\beta_{m,k}$ [given by Eq. (4)], in order to reproduce these modes amplitudes by Eq. (32):

$$A_{j,k} = \frac{1}{\sqrt{M+1}} \sum_{m=1}^{M} \sin mq_j \left(-\mathrm{e}^{-i\varphi_{j,k}} \alpha_{m,k} + \mathrm{e}^{i\varphi_{j,k}} \beta_{m,k} \right),$$

$$A_{-j,k} = \frac{1}{\sqrt{M+1}} \sum_{m=1}^{M} \sin mq_j \left(\mathrm{e}^{-i\varphi_{j,k}} \alpha_{m,k} + \mathrm{e}^{i\varphi_{j,k}} \beta_{m,k} \right). \quad (45)$$

Using these operators, the GF matrix elements can be considered in the more general framework of two-time GF's [19, 20] as:

$$\left\langle \langle A_{j,k} \mid A_{j',k'}^{\dagger} \rangle \right\rangle (\varepsilon) = \frac{1}{\pi} \int_0^{\infty} dt \mathrm{e}^{it(\varepsilon - i0)} \left\langle \left\{ A_{j,k}(t), A_{j,k}^{\dagger}(0) \right\} \right\rangle \quad (46)$$

with the Heisenberg picture operators $A(t) = \mathrm{e}^{iH^{(a,M)}t} \times$ $\times A \mathrm{e}^{-iH^{(a,M)}t}$ under anti-commutator $\{.,.\}$ and quantum-statistical average $\langle \ldots \rangle$. In particular, it gives $G_{j,j}^{(a,M)} \equiv$ $= \langle \langle A_{j,k} \mid A_{j',k'}^{\dagger} \rangle \rangle$.

Then the orthogonality relation:

$$\frac{1}{M+1} \sum_{j=1}^{M} \sin mq_j \sin m'q_j = \delta_{m,m'}, \quad (47)$$

permits also the inverse expansions of position operators:

$$\alpha_{m,k} = \frac{1}{\sqrt{M+1}} \sum_{j=1}^{M} \sin mq_j \mathrm{e}^{i\varphi_{j,k}} A_{j,k}^{(-)},$$

$$\beta_{m,k} = \frac{1}{\sqrt{M+1}} \sum_{j=1}^{M} \sin mq_j \mathrm{e}^{-i\varphi_{j,k}} A_{j,k}^{(+)}, \quad (48)$$

in symmetric and antisymmetric combinations of eigenmode operators $A_{j,k}^{(\pm)} = A_{-j,k}^{(+)} \pm A_{j,k}^{(-)}$. The latter expansions are just helpful for treating the AGNR perturbations from local impurity centers.

5. Impurity perturbations

5.1. Zigzag edge modes

Focusing on the impurity effects in ZGNR on its most interesting edge modes, we begin it in the framework of the simplest Lifshitz perturbation model, where the perturbation Hamiltonian:

$$H_{\mathrm{L}}' = V \sum_p a_{1,p}^{\dagger} a_{1,p} \quad (49)$$

is restricted to the substitutional impurities at a type sites in the 1st chain (in mind to add the same effect from impurities at b type sites in Mth chain). Here V is the local atomic energy shift on carbon atom belonging to the sublattice a that is located at a random pth segment within the 1st chain and we assume the concentration of such perturbed sites small: $c = N^{-1} \sum_p 1 \ll 1$.

Then the perturbed dispersion equation for the edge mode includes the self-energy term that can be written in the T matrix approximation as follows:

$$\varepsilon - \mathrm{Re} \frac{cV}{1 - V g_M(\varepsilon)} - \varepsilon_{1,k} = 0. \quad (50)$$

In the above expression $g_M(\varepsilon)$ stands for the ZGNR locator function:

$$g_M(\varepsilon) = \frac{1}{2\pi} \int_0^{2\pi} G_{1,1}^{(z,M)}(k) dk \quad (51)$$

(taking account of both conduction and valence edge modes). Using Eqs. (43), (51), and the approximated dispersion law, Eq. (23), we present it as:

$$g_M(\varepsilon) \approx \frac{1}{\varepsilon} \int_0^1 \frac{dx}{1 - (u_\varepsilon x)^{2M}}, \quad (52)$$

with $u_\varepsilon = \pi / \varepsilon^{1/M}$. The latter integral is expressed analytically:

$$\int_0^1 \frac{dx}{1-(u_\varepsilon x)^{2M}} = {}_2F_1\left(1, \frac{1}{2M}; 1+\frac{1}{2M}; u_\varepsilon{}^{2M}\right), \quad (53)$$

as the hypergeometric function ${}_2F_1$ [25]. Its asymptotics at low enough energies, $\varepsilon^{1/M} \lesssim 1$ hence $u_\varepsilon \gtrsim 1$, reads:

$${}_2F_1\left(1, \frac{1}{2M}; 1+\frac{1}{2M}; u_\varepsilon{}^{2M}\right) \approx \frac{1}{u_\varepsilon},$$

which provides a simple approximation for the locator function:

$$g_M(\varepsilon) \approx \frac{1}{\pi\varepsilon^{1-1/M}}\left(1-\frac{i\pi}{2M}\right), \quad (54)$$

being of the order $\sim 1/\varepsilon \gg 1$ and dominated by its real part. Note this behavior to be in a striking contrast with that for the limit of a single isolated zigzag chain (1 nanoribbon):

$$g_1(\varepsilon) = \frac{\varepsilon}{\pi}\int_0^\pi \frac{dk}{\varepsilon^2-\gamma_k^2} \approx \frac{i}{2} + \frac{\varepsilon}{\pi^2}, \quad (55)$$

being dominated by its imaginary part of the order ~ 1.

When the result of Eq. (54) is used in the dispersion equation, Eq. (50) (supposing $|V| \sim 1$), it defines the impurity perturbation of the edge mode, and this turns to be very weak, $\varepsilon_{1,k} \to \varepsilon_{1,k} - \Delta_{1,k}$, where:

$$\Delta_{1,k} \approx \pi c \varepsilon_{1,k}^{1-2/M} \ll \varepsilon_{1,k}. \quad (56)$$

Along with this small energy shift, there also emerges yet smaller inverse lifetime: $\hbar\tau_k^{-1} \sim c\varepsilon_{1,k}/M \ll \Delta_{1,k}$, both effects resulting in fact negligible. This analysis explains the microscopic mechanism for the topological protection of the zigzag edge states.

From another perspective (e.g., impurity adatoms instead of substitution impurities), the impurity effect on the edge modes can be considered within the Anderson hybrid model. Therein, an adatom impurity (described by its Fermi operator c_p) at a random point p becomes characterized by its energy level ε_0 and its hybridization ω with a type (or b type, on the opposite edge) carbons in its nearest neighbor vicinity.

Two possible impurity positions with respect to the ribbon edge can be indicated: (a) top position [Fig. 4(a)] when the impurity is hybridizing with a single carbon atom from the edge chain, and (b) bridge position [Fig. 4(b)] when the impurity sets symmetrically between two neighboring a type host atoms. This generates the perturbation Hamiltonian:

$$H'_A = \sum_p \left(\varepsilon_0 c_p^\dagger c_p + \frac{\omega}{\sqrt{N}}\sum_{k,\delta} e^{ik(p+\delta)} c_p^\dagger a_1(k) + \text{h.c.}\right), \quad (57)$$

where δ is an impurity separation from a neighboring host site, measured along the edge. In the top case (a), we set $\delta = 0$ in Eq. (57) and the T matrix approximation for the edge mode dispersion equation takes the form:

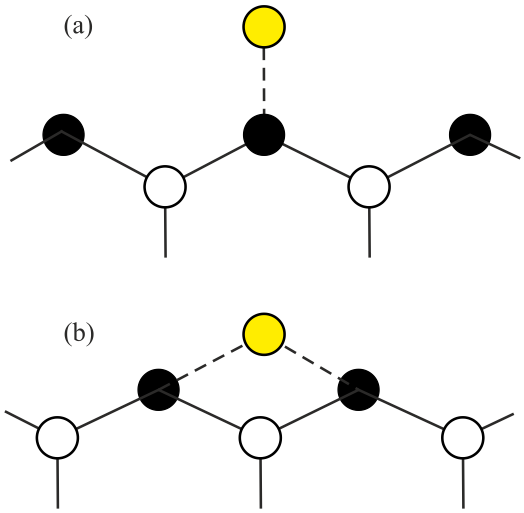

Fig. 4. Different positions of the Anderson impurity near the edge of a graphene ribbon: (a) top position and (b) bridge position.

$$\varepsilon - \frac{c\omega^2}{\varepsilon - \varepsilon_0 - \omega^2 g_M(\varepsilon)} - \varepsilon_{1,k} = 0. \quad (58)$$

Within the same approximation, $g_M(\varepsilon) \approx 1/\varepsilon$, this presents as:

$$\varepsilon - \frac{c\omega^2\varepsilon}{(\varepsilon-\varepsilon_+)(\varepsilon-\varepsilon_-)} - \varepsilon_{1,k} = 0, \quad (59)$$

where

$$\varepsilon_\pm = \frac{\varepsilon_0 \pm \sqrt{\varepsilon_0^2+4\omega^2}}{2}.$$

Then, considering the lowest energy range, $\varepsilon^2 \sim \varepsilon_{1,k}^2 \ll \varepsilon_\pm^2$, this simplifies to:

$$\varepsilon(1+c) - \varepsilon_{1,k} = 0,$$

showing the same extremely weak perturbation of the edge mode as in the Lifshitz model.

Finally, for the bridge position of impurity, the case (b), the T matrix is built from the scattering amplitudes, $\Omega_k = \omega\gamma_k$, and takes the form:

$$T_k = \frac{\Omega_k^2}{\varepsilon - \varepsilon_0 - \omega^2 \tilde{g}_M(\varepsilon)}, \quad (60)$$

with the modified locator function

$$\tilde{g}_M(\varepsilon) = \frac{\varepsilon}{\pi}\int_0^\pi \frac{\gamma_k^2 dk}{\varepsilon^2-\varepsilon_{1,k}^2}.$$

In similarity to Eq. (51), this locator is approximated as:

$$\tilde{g}_M(\varepsilon) \approx \frac{\pi^2}{3\varepsilon}\,{}_2F_1\left(1, \frac{1}{3M}; 1+\frac{1}{3M}; u_\varepsilon{}^{2M}\right), \quad (61)$$

and from the corresponding asymptotics at $u_\varepsilon \gtrsim 1$:

$${}_2F_1\left(1, \frac{1}{2M}; 1+\frac{1}{2M}; u_\varepsilon{}^{2M}\right) \approx \frac{1}{u_\varepsilon^{2/3}},$$

we find it as:

$$\tilde{g}_M(\varepsilon) \approx \frac{1}{\varepsilon^{1-2/(3M)}}\left(\frac{\pi^{4/3}}{3} + i\frac{\varepsilon^{7/(3M)}}{2M}\right), \qquad (62)$$

that is again of the order $\sim 1/\varepsilon$ and dominated by its real part. Using this result in the dispersion equation, Eq. (58), we obtain the impurity effect as $\Delta_k \approx (3/\pi^{4/3})c\varepsilon^{1+4/(3M)}$, even weaker than for the above considered Lifshitz or Anderson-top cases.

All the considered examples of impurity perturbations suggest that the topological protection from disorder is quite a universal property of the zigzag edge modes.

5.2. Armchair Dirac-like modes

Turning to the AGNR spectrum, we again focus on its lowest Dirac-like modes at a proper nanoribbon width, $M = 3r-1$. For simplicity, we restrict the analysis to the Lifshitz model expressed in the relevant $A_{\pm r,k}$ operators as:

$$H'_{\rm L} = \frac{2V}{3rN}\sum_p{}' \sum_{k,k'} e^{ip(k-k')} e^{i(\varphi_{r,k}-\varphi_{r,k'})} \times$$

$$\times\left(A^{\dagger}_{-r,k} - s_p A^{\dagger}_{r,k}\right)\left(A_{-r,k'} - s_p A_{r,k'}\right), \qquad (63)$$

where $\sum_p{}'$ is restricted to only impurity cites p from odd chains and $s_p = \pm 1$ for p being of a or b type, repectively. This Hamiltonian generates a perturbation of the GF matrix $\hat{G}^{(a,M)} \to \hat{\tilde{G}}^{(a,M)}$, the latter being defined in the T matrix approximation as:

$$\left(\hat{\tilde{G}}^{(a,M)}\right)^{-1} = \left(\hat{G}^{(a,M)}\right)^{-1} - c\hat{T}.$$

It involves the 2×2-fold T matrix in the basis of Dirac-like states, $\{\varphi_{r,k}, \varphi_{-r,k}\}$ (at each given k): $\hat{T} = (\hat{1} - s_p\hat{\sigma}_1)T$, with the Pauli matrix $\hat{\sigma}_1$ and the scalar $T = cV/[1-Vg_1]$ where the locator is just that by Eq. (55), $g_1 \approx i/2$. Then the modified dispersion laws follow from the standard GF secular equation [26], $\mathrm{Re}\,[\det(\hat{\tilde{G}}^{(a,M)})^{-1}] = 0$, as:

$$\tilde{\varepsilon}_{\pm r,k} = \pm\sqrt{\varepsilon^2_{r,k} + (c\,\mathrm{Re}T)^2} + c\,\mathrm{Re}T, \qquad (64)$$

but their validity should be checked with the Ioffe–Regel–Mott (IRM) criterion [27, 28]:

$$k\frac{\partial}{\partial k}\tilde{\varepsilon}_{\pm r,k} \gtrsim c\,\mathrm{Im}T. \qquad (65)$$

The condition that the IRM criterion fails gives an estimate for the width of the mobility gap around zero energy:

$$\Delta_m \sim cf(V), \qquad (66)$$

where the function

$$f(V) = \frac{V^2}{4+V^2}\sqrt{2\left(1+\sqrt{1+(4/V)^2}\right)}$$

grows with the perturbation strength as $f(V) \approx |V|^{3/2}/2$ at $|V| \ll 1$ up to $f(V) \approx 2$ at $|V| \gg 1$.

The result by Eq. (66) defines the most important impurity effect on the AGNR Dirac-like modes — all the modes with eigenenergies within $|\varepsilon| < \Delta_m$ are localized on impurity centers while the modes outside this range stay conductive, which should produce metal/insulator transitions if the Fermi level crosses the corresponding mobility edges, $|\varepsilon| = \Delta_m$ (either from conduction or valence side).

The same considerations can be also developed for other impurity models but they will not change the qualitative result of the above Lifshitz model.

The above analysis underlines again the differences between the two GNR types, here in the AGNR high sensitivity to the impurity disorder (vs the ZGNR topological protection), then in its specific sensitivity to the atomically defined width of a nanoribbon and, at last, to the parity of the numbers of atomic chains where impurities reside.

6. Discussion

The obtained results demonstrate how the difference of electronic states in graphene nanoribbons defined by their edge orientations is reflected in their stability against impurity disorder. Physically, this opens the possibility for specific electronic phase transitions and for their controls, e.g., by combining the disorder and external bias effects. The present study was limited to the simplest framework of tight-binding model for pure nanoribbons and the simplest models for impurity perturbations on them. In principle, it can be extended to account for many other physical factors, as electron-electron Hubbard correlations, different types of spin-orbit coupling, spin-ordering effects, external electric and magnetic biases, finite temperatures, and so on. Also, the effects from passivating hydrogens, known to be commonly present at the edges of experimental nanoribbon samples, may influence the dynamics of host nanoribbon carriers. This factor can be naturally included into the above developed recursive algorithms and resulting Green functions, to be possibly an object of future study. At the very least, the experimental testing of intended effects, such as the mobility of carriers and their collapse in certain directions, should be of considerable interest.

Acknowledgments

The work of VML was partially supported by the Ukrainian–Israeli Scientific Research Program of the Ministry of Education and Science of Ukraine and the Ministry of Science and Technology of the State of Israel, as well as by Grant Nos. 0117U000236 and 0117U000240 from the Department of Physics and Astronomy of the National Academy of Sciences of Ukraine. DK acknowledges support from Deutsche Forschungsgemeinschaft, Project-ID 314695032 (SFB 1277), and the EU Seventh Framework Programme under Grant Agreement No. 604391 (Graphene Flagship). The authors appreciate the fruitful discussions of various aspects of the present problem with Dr. J. Fabian, Dr. A. Ferreira, and Dr. J. M. V. P. Lopes.

1. F. Wudle, *Fullerene materials*, *J. Mater. Chem.* **12**, 1959 (2002).
2. S. Iijima, *Carbon Nanotubes, Past, Present, and Future*, *Physica B* **323**, (2002).
3. H. P. Boehm, A. Clauss, G. O. Fischer, and U. Hofmann, *Das Adsorptionsverhalten Sehr Dünner Kohlenstoff-folien*, *Z. Anorg. Allg. Chem.* **316**, 119 (1962).
4. K. S. Novoselov, A. K. Geim, S. V. Morozov, S. V. Dubonos, Y. Zhang, and D. Jiang, *Room-temperature Electric Field Effect and Carrier-type Inversion in Grapheme Films*, *arXiv*, *cond-mat/0410631* (2004).
5. S. V. Morozov, K. S. Novoselov, F. Schedin, D. Jiang, A. A. Firsov, and A. K. Geim, *Two-dimensional Electron and Hole Gases at the Surface of Graphite*, *Phys. Rev. B* **72**, 201401 (2005).
6. A. H. Castro Neto, F. Guinea, N. M. R. Peres, K. S. Novoselov, and A. K. Geim, *The Electronic Properties of Graphene*, *Rev. Mod. Phys.* **109**, 109 (2009).
7. M. Inagaki and F. Kang, *Graphene Derivatives, Graphane, Fluorographene, Graphene oxide, Graphyne and Graphdiyne*, *J. Mater. Chem. A* **2**, 13193 (2014).
8. D. Tománek, *Guide Through the Nanocarbon Jungle*, Morgan & Claypool Publishers (2014), pp. 2053-2571.
9. L. Brey and H. A. Fertig, *Edge States and the Quantized Hall Effect in Graphene*, *Phys. Rev. B* **73**, 195408 (2006).
10. P. M. Perez-Piskunow, G. Usaj, C. A. Balseiro, and L. E. F. Foa Torres, *Floquet Chiral Edge States in Graphene*, *Phys. Rev. B* **89**, 121401 (2014).
11. M. C. Rechtsman, Y. Plotnik, J. M. Zeuner, D. Song, Z. Chen, A. Szameit, and M. Segev, *Topological Creation and Destruction of Edge States in Photonic Graphene*, *Phys. Rev. Lett.* **111**, 103901 (2013).
12. J. L. Lado, N. García-Martínez, and J. Fernández-Rossier, *Edge States in Graphene-like Systems*, *Synth. Met.* **210**, 56 (2015).
13. P. Qiu, R. Liang, W. Qiu, H. Chen, J. Ren, Z. Lin, J.-X. Wang, Q. Kan, and J.-Q. Pan, *Topologically Protected Edge States in Graphene Plasmonic Crystals*, *Opt. Express* **25**, 22587 (2017).
14. T. Frank, P. Högl, M. Gmitra, D. Kochan, and J. Fabian, *Protected Pseudohelical Edge States in Z_2-trivial Proximitized Graphene*, *Phys. Rev. Lett.* **120**, 156402 (2018).
15. M. Fujita, K. Wakabayashi, K. Nakada, and K. Kusakabe, *Peculiar Localized State at Zigzag Graphite Edge*, *J. Phys. Soc. Jpn.* **65**, 1920 (1996).
16. K. Wakabayashi, Y. Takane, M. Yamamoto, and M. Sigrist, *Electronic Transport Properties of Graphene*, *New J. Phys.* **11**, 095016 (2009).
17. K. Wakabayashi, K. Sasaki, T. Nakanishi, and T. Enoki, *Electronic States of Graphene Nanoribbons and Analytical Solutions*, *Sci. Technol. Adv. Mater.* **11**, 054504 (2010).
18. W. F. da Cunha, A. Ribeiro, A. L. de Almeida Fonseca, R. Gargano, and G. M. e Silva, *Impurity Effects on Polaron Dynamics in Graphene Nanoribbons*, *Carbon* **91**, 171 (2015).
19. D. Zubarev, *Double-time Green Functions in Statistical Physics*, *Sov. Phys. Usp.* **3**, 320 (1960).
20. E. N. Economou, *Green's Functions in Quantum Physics*, Springer (1979).
21. S. Irmer, D. Kochan, J. Lee, and J. Fabian, *Resonant Scattering Due to Adatoms in Graphene, Top, Bridge, and Hollow Positions*, *Phys. Rev. B* **97**, 075417 (2018).
22. Y. G. Pogorelov, V. M. Loktev, and D. Kochan, *Impurity Resonance Effects in Graphene Versus Impurity Location, Concentration, and Sublattice Occupation*, *Phys. Rev. B* **102**, 155414 (2020).
23. M. I. Kaganov and I. M. Lifshitz, *Electron Theory of Metals and Geometry*, *Sov. Phys. Usp.* **22**, 904 (1979).
24. M. I. Kaganov, *Energy Spectrum of a Metal and its Singularities*, *Sov. Phys. Usp.* **28**, 257 (1985).
25. M. Abramowitz and I. Stegun, *Handbook of Mathematical Functions*, National Bureau of Standards (1964).
26. V. L. Bonch-Bruevich and S. V. Tyablikov, *The Green Function Method in Statistical Mechanics*, North Holland Publishing House (1962).
27. A. F. Ioffe and A. R Regel, *Non-crystalline, Amorphous and Liquid Electronic Semiconductors*, *Progress Semicond.* **2**, 237 (1960).
28. N. F. Mott, *Conduction in Non-crystalline Materials III. Localized States in a Pseudogap and near Extremities of Conduction and Valence Bands*, *Phil. Mag.* **102**, 835 (1962).

Електронні спектри, топологічні стани та домішкові ефекти в нанострічках графену

Yuriy G. Pogorelov, Denis Kochan, Vadim M. Loktev

Розглянуто обмежені стрічки графену з двома основними орієнтаціями їхніх бокових країв, «зигзаг» та «крісло», для детального вивчення впливу домішок на їхні крайові стани. Альтернативою до відомого опису їхніх спектрів у термінах стійних поперечних хвиль запропоновано рекурентні співвідношення спектрів від дискретних чисел атомарних ланцюжків у стрічці, що уможливлює спрощення опису функціями Гріна ефектів розупорядкування в цих системах. Здійснений аналіз показує мікроскопічні механізми збурення різними типами домішок низькоенергетичних станів і висвітлює, як стабільність топологічних станів до розупорядкування у «зигзаг» системах пов'язується із дискретними амплітудами цих станів упоперек стрічки. Навпаки, можливість моттовської локалізації під впливом домішкового збурення знайдено для нанострічок типу «крісло», але тільки для особливих значень їхньої ширини.

Ключові слова: графенові нанострічки, топологічні стани, домішковий розлад, модель Ліфшиця, модель Андерсона.